# Assessment of Voltage Sag Indices Based on Scaling and Wavelet Coefficient Energy Analysis

Flavio B. Costa, *Member, IEEE*, and Johan Driesen, *Senior Member, IEEE*

***Abstract*—The two main voltage sag indices are magnitude and duration, defined in terms of the well-known rms voltages. The spectral energy of the voltages provides the same voltage sag indices of the rms voltage analysis and less computational effort is required. However, neither of them provide point on wave of sag initiation and recovery. This paper presents a wavelet-based methodology for the characterization of voltage sags, where the spectral energy of a voltage is decomposed in terms of the scaling and wavelet coefficient energies. The scaling coefficient energies of the phase voltages are used for voltage sag characterization, providing sag indices (magnitude and duration) in agreement with the definition. However, the analysis of the wavelet coefficient energies of such voltages provides additional information for the identification of the point on wave of voltage sag initiation and recovery as well as important parameters for power system protection and voltage sag mitigation devices. The performance of the proposed wavelet-based methodology was assessed with actual data and it was scarcely affected by the choice of the mother wavelet. Therefore, a compact mother wavelet can be used for voltage sag analysis with computational effort equivalent to the rms method and in agreement with practical applications. The maximal overlap discrete wavelet transform presented better performance than the discrete wavelet transform. All of the equations provided in this paper were developed for real-time analysis.**

***Index Terms*—High-speed sag detection, voltage sag indices, wavelet transform.**

## I. Introduction

VOLTAGE SAGS are currently one of the main power-quality (PQ) issues, defined by a short-duration reduction in rms voltage, caused by the short-duration increase in currents due to faults, overloads, and the starting of large motors [1]. Faults are the main causes of voltage sags.

The residual voltage (the rms voltage magnitude as a percentage of a reference voltage during the event) and duration are the two main indices for voltage sag characterization [2]. An accurate estimation of these parameters is important to help system designers select appropriate equipment specifications for critical processes. The well-known conventional procedure for voltage sag characterization is based on the analysis of rms voltages over a window equal to one cycle of the power system frequency [3]. Though very simple and efficient, rms-based methods can provide errors in estimation of some event characteristics. For instance, the rms voltage does not immediately drop to a lower value, but takes a while during the transition, and the rms voltage does not immediately recover after the fault [2], which can lead to errors in estimation of the point on wave of sag initiation and recovery. Limitations associated with rms methods are discussed in [4].

The spectral energy of phase voltages can be properly used for voltage sag characterization with exactly the same performance of rms-based methods when the reference voltage is obtained during the steady-state operation. The advantage of the energy-based analysis is the less computational effort in real-time applications. However, this procedure presents the same drawbacks of the conventional rms method.

The transition between presag and during-sag voltage contains a large amount of higher frequency components [1], termed as transients in this paper. The analysis of transients can provide an accurate identification of the point on wave of sag initiation and recovery. This information may be used for network operators to improve their supply. The performance of some equipment used for mitigating sags also depends on the detection of the point on wave of sag initiation [2].

The discrete wavelet transform (DWT) and its variant, the maximal overlap discrete wavelet transform (MODWT), decompose a sampled signal in time into scaling and wavelet coefficients. The well-known application of the wavelet coefficients is to detect and classify PQ disturbances [5]. For instance, the start and end time of voltage sags can be identified by means of the wavelet coefficient analysis [6], [7]. However, the wavelet coefficients are quite influenced by the mother wavelet. An interesting feature of the wavelet transform is its energy conservation principle, where the spectral energy of a signal can be decomposed into the scaling and wavelet coefficient energies. The wavelet coefficient energies of the DWT [8], [9] and MODWT [10] have also been used for fault and some PQ disturbance detection.

This paper presents a new methodology to compute the scaling and wavelet coefficient energies of the wavelet transform, instead of the spectral energy analysis, as a fast and efficient tool for voltage sag characterization. The scaling coefficient energy analysis provides sag indices (magnitude and duration) in accordance with the definition with processing time equivalent to the rms voltage computation. However, the

Manuscript received March 09, 2012; revised July 15, 2012; accepted September 08, 2012. Date of publication October 24, 2012; date of current version December 19, 2012. This work was supported in part by the Brazilian National Research Council (CNPq), Coimbra Group, and in part by K. U. Leuven. Paper no. TPWRD-00248-2012.

F. B. Costa is with Federal University of Rio Grande do Norte—School of Science and Technology, Campus Univesitário Lagoa Nova, Natal 59.078-970, Brazil (e-mail: flaviocosta@ect.ufrn.br).

J. Driesen is with the Electrical Engineering Department ESAT-ELECTA, K. U. Leuven, Heverlee B-3001, Belgium (e-mail: Johan.Driesen@esat.kuleuven.be).

Color versions of one or more of the figures in this paper are available online at http://ieeexplore.ieee.org.

Digital Object Identifier 10.1109/TPWRD.2012.2218626

wavelet coefficient energies can be used for high-speed detection of sags, providing additional point on wave of sag initiation and recovery more effectively than the well-known wavelet coefficient analysis. The extraction of sag indices by means of the proposed wavelet-based energies is almost not highly influenced by the choice of the mother wavelet. In addition, the MODWT provides better performance than the DWT.

Several wavelet-based methods for PQ disturbance analysis have been developed. Notwithstanding, the performance evaluation of these methods with actual data has been small. The extraction of the voltage sag indices obtained through the proposed wavelet-based methodology was compared to the conventional rms-based method by using actual records with voltage sags. This performance assessment with actual data will be vital for further development of voltage sag detection methods to yield results in satisfactory agreement with practical applications. In addition, all of the wavelet-based equations were developed for real-time applications.

## II. Energy of the Real-Time MODWT

Both the DWT and MODWT use low- and high-pass filters (scaling and wavelet filters) to divide the frequency band of the input signal into scaling and wavelet coefficients, respectively. The scaling $(g)$ and wavelet $(h)$ filters are quadrature mirror filters of length $L$ (even number) associated with the selected mother wavelet, which divides the frequency spectrum of the original signal into octave bands. As a consequence, at the first scale, it is well-known that:

- the scaling coefficients $(s)$ are mainly influenced by the smallest frequency components of the original signal, from dc to $f_s/4$, where $f_s$ is the sampling frequency; in case of voltage sag data obtained through a typical digital fault recorder with $f_s = 15.36$ kHz, these coefficients may preserve information regarding the fundamental power frequency;
- the wavelet coefficients $(w)$ are mainly influenced by the highest frequency components of the signal, from $f_s/4$ to $f_s/2$, which can be properly used for high-speed detection of the transients at the point on wave of sag initiation and recovery [6].

In contrast to the DWT, there is no downsampling in MODWT [11]. Therefore, transients induced by faults as well as transients in voltage sags can be detected faster by means of the MODWT [12]. In this paper, $s$ and $w$ are computed through the MODWT.

By using the MODWT pyramid algorithm, all samples of the signal, which are intended to be analyzed (main window), are required to compute $s$ and $w$. The first $L-1$ coefficients may present border distortions because their computation is accomplished with samples at the beginning and end of the main window [11].

The scaling and wavelet coefficients of the MODWT can also be computed in real time by using a modification of the pyramid algorithm [12], as follows:

$$s(k) = \sum_{l=1}^{L} \tilde{g}(l) v(k+l-L), \tag{1}$$

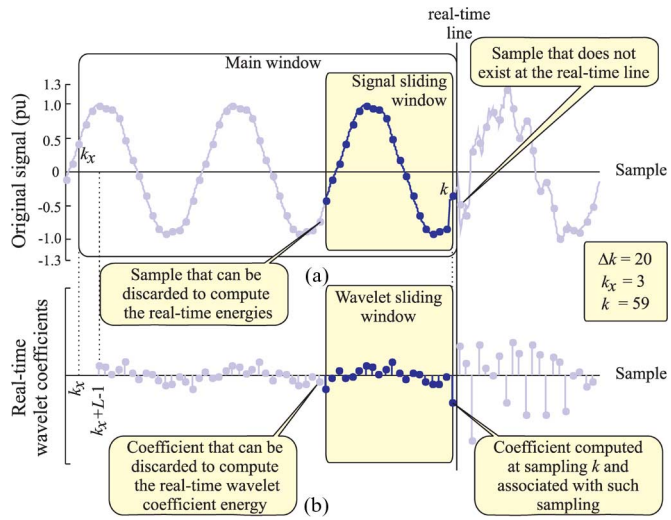


Fig. 1. Real-time computation of the wavelet coefficients of the MODWT. (a) Original signal. (b) Real-time wavelet coefficients $w$.

$$w(k) = \sum_{l=1}^{L} \tilde{h}(l) v(k+l-L) \tag{2}$$

where $k \geqslant k_x + L - 1$ occurs once the last samples of the original signal $(v)$ are not available, and the first $L-1$ coefficients, which would be affected by border effects in the conventional pyramid algorithm, cannot be computed in real time; $k$ corresponds to the last sampling; $k_x$ is the first sample of the original signal taken into consideration to compute $s$ and $w$; and $\tilde{g}(i) = g(i)/\sqrt{2}$ and $\tilde{h}(i) = h(i)/\sqrt{2}$. The processing time has to be accomplished into $1/f_s$ seconds.

The scaling and wavelet coefficients of the DWT can also be computed in real time by means of inner products of $g$ and $h$ with the last $L$ samples of $v$, respectively. Therefore, in real-time applications, the time consumption to compute these coefficients is the same as the MODWT. However, due to the downsampling process, the real time $s$ and $w$ of the DWT are computed only in alternate samplings, whereas $s$ and $w$ of the MODWT are computed in every sampling.

Fig. 1 depicts the process to compute the real-time wavelet coefficient $w$ of the MODWT by using the Daubechies wavelet with four coefficients (db(4)). The original signal is a sampled version with $f_s = 1200$ Hz of an actual signal with transients. From $k_x$ in real time, $k$ is always the last sample of the main window (last signal sampling), increasing when the real-time line reaches a new sampling. In this case, $k$ is the first sample with transients.

It is well known that each scaling and wavelet coefficient is located in time at the midpoint of the $L$ samples of the original signal that originated such coefficients by means of an inner product with $g$ and $h$, respectively [11]. In real time, however, $s$ and $w$ of the MODWT are computed at sample $k$ with the last $L$ samples of the signal, and these coefficients are associated with the $k$th sampling. Therefore, a delay of the real-time scaling and wavelet coefficients regarding the coefficients of the conventional pyramid algorithm is expected.

The spectral energy ($\mathcal{E}$) of a window of length $\Delta k$ sliding in the real-time voltage (signal sliding window) is given by

$$\mathcal{E}(k) = \sum_{m=k-\Delta k+1}^{k} v^2(m) \tag{3}$$

where $k \geqslant k_x + \Delta k - 1$ and $\mathcal{E} = \{\mathcal{E}_{v_A}, \mathcal{E}_{v_B}, \mathcal{E}_{v_C}\}$ are the energies of the voltages $v = \{v_A, v_B, v_C\}$, respectively. In this paper, $\Delta k = f_s/f$ is equal to one cycle of the power frequency ($f$).

According to the theorem of Parseval, the energy of a signal can be decomposed in terms of the energy of scaling and wavelet coefficients [11]. In real time, the spectral energy of the signal sliding window (3) can also be decomposed into the scaling coefficient energies ($\mathcal{E}^s$) and the wavelet coefficient energies ($\mathcal{E}^w$), at the first scale, as follows:

$$\mathcal{E}(k) = \mathcal{E}^s(k) + \mathcal{E}^w(k) \tag{4}$$

where $\mathcal{E}^s$ and $\mathcal{E}^w$ are proposed to be decomposed into two more components

$$\mathcal{E}^s(k) = \mathcal{E}^{sa}(k) + \mathcal{E}^{sb}(k), \tag{5}$$
$$\mathcal{E}^w(k) = \mathcal{E}^{wa}(k) + \mathcal{E}^{wb}(k) \tag{6}$$

since $k \geqslant k_x + \Delta k - 1$. The energies $\mathcal{E}^s$ and $\mathcal{E}^w$ are computed by means of the scaling sliding window and wavelet sliding window [Fig. 1(b)], which are located at the real-time coefficients $s$ and $w$, respectively.

The components $\mathcal{E}^{sa}$ and $\mathcal{E}^{wa}$ are due to the scaling and wavelet coefficients with border effects of the samples inside the signal sliding window as follows:

$$\mathcal{E}^{sa}(k) = \sum_{n=1}^{L-1} \tilde{s}^2(n), \tag{7}$$
$$\mathcal{E}^{wa}(k) = \sum_{n=1}^{L-1} \tilde{w}^2(n) \tag{8}$$

since $k \geqslant k_x + \Delta k - 1$. Instead of the first $L-1$ real-time coefficients of the scaling and wavelet sliding windows, which are not affected by border effects of the samples of the voltage sliding window, the coefficients with border effects $\tilde{s}$ and $\tilde{w}$ are used to compute $\mathcal{E}^{sa}$ and $\mathcal{E}^{wa}$, respectively. These $L-1$ coefficients are computed as follows:

$$\tilde{s}(n) = \sum_{l=1}^{L} \tilde{g}(l)\tilde{v}(n+l-1), \tag{9}$$
$$\tilde{w}(n) = \sum_{l=1}^{L} \tilde{h}(l)\tilde{v}(n+l-1) \tag{10}$$

where $n = 1, 2, \ldots, L-1$ and $\tilde{v} = \{\tilde{v}(1), \tilde{v}(2), \ldots, \tilde{v}(2L-2)\} = \{v(k-L+2), v(k-L+3), \ldots, v(k), v(k-\triangle k+1), \ldots, v(k-\triangle k+L-1)\}$ is a sequence of the last $L-1$ and the first $L-1$ samples of the signal sliding window.

The components $\mathcal{E}^{sb}$ and $\mathcal{E}^{wb}$ are computed with the real-time scaling and wavelet coefficients, as follows:

$$\mathcal{E}^{sb}(k) = \sum_{n=k-\Delta k+L}^{k} s^2(n) \tag{11}$$
$$\mathcal{E}^{wb}(k) = \sum_{n=k-\Delta k+L}^{k} w^2(n) \tag{12}$$

since $k \geqslant k_x + \Delta k - 1$. The first $L-1$ coefficients of the scaling and wavelet sliding windows are not taken into account.

The scaling and wavelet coefficient energies were defined by [10] as follows:

$$\ddot{\mathcal{E}}(k) = \sum_{n=k-\Delta k+1}^{k} s^2(n) \tag{13}$$
$$\dot{\mathcal{E}}(k) = \sum_{n=k-\Delta k+1}^{k} w^2(n) \tag{14}$$

since $k \geqslant k_x + \Delta k + L - 2$. These energies take into account all real-time coefficients into the scaling and wavelet sliding windows, respectively. Therefore, the coefficients with border effects of the signal sliding window are not taken into account. As a consequence, $\mathcal{E} \neq \dot{\mathcal{E}} + \ddot{\mathcal{E}}$.

## III. Characterization of Voltage Sag

The IEEE Standards 1159-1995 [13] and IEC 61000-4-30 [3] are the two main standards that define voltage sag (dip), swell, and interruption. In this paper, based on these standards, voltage sags, swells, and interruptions are characterized by their magnitude (rms value) and duration as follows.

- The voltage sag starts when at least one of the rms voltages drops below the threshold of 90% of the reference voltage and ends when all three rms voltages have been recovered above this threshold for durations from half-cycle to 1 min.
- The voltage swell starts when at least one of the rms voltages rises above the threshold of 110% of the reference voltage and ends when all three rms voltages have been recovered below this threshold for durations from half cycle to 1 min.
- Voltage interruption starts when all three rms voltages drop below the threshold of 10% of the reference voltage and ends when at least one of them rises above this threshold for durations from half cycle to 1 min.

Voltage sags are mainly due to faults [1]. Only voltage sags will be properly dealt with in this paper. However, the analysis accomplished here can be extended for voltage swell and interruption characterization.

### A. RMS-Based Analysis

The IEC PQ measurement standard 61000-4-30 [3] prescribes a precise rms-based method for obtaining the voltage magnitude as a function of time. In fact, most commonly used PQ monitors calculate not the fundamental component but the rms value over a one-cycle or half-cycle window of the power system frequency [2]. The calculation of the one-cycle rms

voltage can be repeated every half-cycle [3]. However, in this paper, the rms voltage $(v_{rms})$ is obtained over a one-cycle window sliding sample by sample in time (voltage sliding window), as follows:

$$v_{rms}(k) = \sqrt{\frac{1}{\Delta k} \sum_{m=k-\Delta k+1}^{k} v^2(m)} \tag{15}$$

where $k > k_x + \Delta k - 1$; the $k$th rms value is associated with the sample $k$ and $v_{\rm rms} = \{v_{\rm Arms}, v_{\rm Brms}, v_{\rm Crms}\}$ are the rms voltages of $v = \{v_A, v_B, v_C\}$, respectively.

Typically, the nominal voltage is used as a reference. However, the voltage at a specific point of the system varies with the time of day. In practical applications, the average voltage over a shorter or longer period, computed many times along the day, is used as a reference voltage $(V)$. In this paper, actual records with voltage sags are assessed and a period of one cycle $(\Delta k)$ before the event is used to compute $V$ as follows:

$$V = \frac{1}{\Delta k} \sum_{m=k_i-\Delta k+1}^{k_i} v_{rms}(m) \tag{16}$$

where $k_i \geqslant k_x + 2\Delta k - 2$; $V = \{V_A, V_B, V_C\}$ are the average values in one cycle of the rms voltages $v_{rms} = \{v_{Arms}, v_{Brms}, v_{Crms}\}$, respectively. The system has to be in steady-state operation at least in two cycles before the sample $k_i$.

The most commonly used methods compare the rms voltages with thresholds and a voltage sag can be confirmed if

$$V_1 V \leqslant v_{rms} \leqslant V_2 V \tag{17}$$

for more than a half-cycle; $V_1 = 0.1$ and $V_2 = 0.9$ are rms voltage thresholds. In a case of voltage swell, $v_{\rm rms} \geqslant V_3 V$ for more than a half-cycle, where $V_3 = 1.1$. With regard to the voltage interruption, the voltages tend toward zero and $v_{\rm rms} \leqslant V_1 V$.

The residual voltage $(R_v)$ is defined in this paper as the rms voltage magnitude as a percentage of a reference voltage during the voltage sag as follows:

$$R_v(k) = \frac{v_{rms}(k)}{V} \tag{18}$$

where $R_v = \{R_{vA}, R_{vB}, R_{vC}\}$ are the residual voltages of $v_{\rm rms} = \{v_{\rm Arms}, v_{\rm Brms}, v_{\rm Crms}\}$, respectively.

Fig. 2 depicts the voltages and currents of an actual record with voltage sag due to a single-line-to-ground (SLG) fault upon a parallel line and the respective one-cycle rms voltages as well. At the monitoring point, the fault inception and clearance times were located at samples $k_1$ and $k_2$, respectively.

According to Fig. 2(a), the voltage magnitude in phase C clearly dropped soon after the fault inception at sample $k_1$ to a value of less than the pre-event voltage for about three-and-a-half cycles. After the fault clearance, at sample $k_2$, the voltage came back to about the presag voltage. However, according to standards, voltage sags are referred to as rms events. This means that instead of looking at the instantaneous voltage waveforms, voltage sag initiation and recovery as well as sag duration are

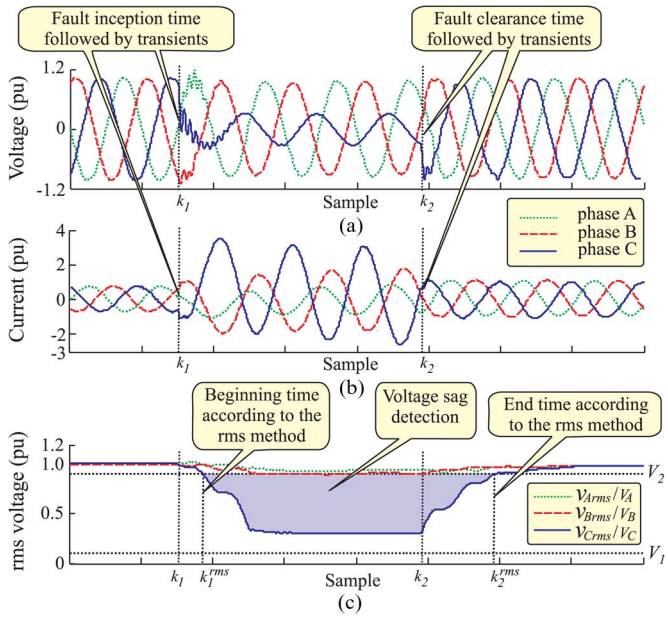


Fig. 2. Actual oscillographic record with a voltage sag due to an SLG fault upon a parallel line. (a) Voltages. (b) Currents. (c) RMS voltages.

obtained through rms voltage analysis. The samples $k_1$ and $k_2$ are defined in this paper as the point on wave of sag initiation and recovery, respectively.

With regard to the rms-based analysis [Fig. 2(c)], from the sample $k_1^{\rm rms}$, the rms voltage related to the faulted phase $(v_{\rm Crms})$ presented a significant drop in magnitude for about four cycles, whereas the other two presented a minor drop. After the fault clearance, the voltage came back to about the presag voltage from the sample $k_2^{\rm rms}$. In this paper, $k_1^{\rm rms}$ and $k_2^{\rm rms}$ are the start and end time of sags obtained through the rms voltage analysis, respectively. The sag duration is given by $k_2^{\rm rms} - k_1^{\rm rms}$.

### B. Spectral Energy-Based Analysis

This paper presents an alternative method to detect voltage sags by means of the one-cycle spectral energy analysis of the voltages, such as those defined in (3). A voltage sag can be detected by comparing $\mathcal{E}(k)$ to a reference energy value $(E)$, which is computed at sample $k_i$ as follows:

$$E = \frac{1}{\Delta k} \sum_{m=k_i-\Delta k+1}^{k_i} \mathcal{E}(m) \tag{19}$$

where $k_i \geqslant k_x + 2\Delta k - 2$, $E = \{E_{v_A}, E_{v_B}, E_{v_C}\}$ are the average values in one cycle of the energies $\mathcal{E} = \{\mathcal{E}_{v_A}, \mathcal{E}_{v_B}, \mathcal{E}_{v_C}\}$, respectively. The system has to be in steady-state operation at least in two cycles before $k_i$.

The rms voltage obtained over a one-cycle window (15) can be defined in terms of the one-cycle voltage energy (3), as follows:

$$v_{\rm rms}(k) = \sqrt{\frac{\mathcal{E}(k)}{\Delta k}}. \tag{20}$$

Taking into consideration $V$ and $E$ computed at the same sample $k_i$, during the steady-state operation, the residual

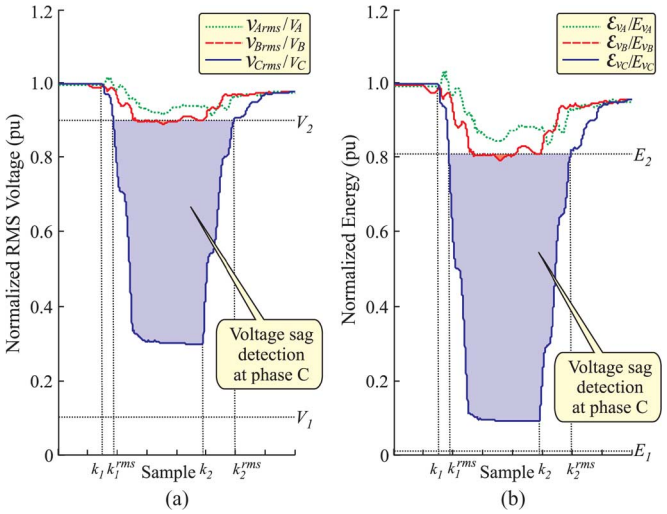


Fig. 3. Voltage sag detection by using: (a) normalized rms voltages and (b) normalized energy voltages.

voltage can be computed as a function of the spectral energy (the Appendix) as follows:

$$R_v(k) \approx \sqrt{\frac{\mathcal{E}(k)}{E}}. \tag{21}$$

By using the spectral energy of the voltage instead of the rms voltage, from (17), a voltage sag can be detected if

$$E_1 E \leqslant \mathcal{E} \leqslant E_2 E \tag{22}$$

for more than a half-cycle; $E_1 = V_1^2 = 0.01$ and $E_2 = V_2^2 = 0.81$ are energy thresholds. Voltage swell and interruption are detected if $\mathcal{E} \geqslant E_3 E$ and $\mathcal{E} < E_1 E$, respectively, where $E_3 = V_3^2 = 1.21$.

Fig. 3 depicts the one-cycle rms voltages and the one-cycle energies regarding the phase voltages shown in Fig. 2, both of which normalized the respective reference voltages and energies obtained during the steady-state system operation. Both of them presented a meaningful signature of the sag.

Exactly the same features presented by the rms voltage were obtained by using the energy of the voltages (Fig. 3). The energy related to the faulted phase ($\mathcal{E}_C$) presented a significant drop in magnitude, whereas the other two presented a minor drop. The residual voltages were the same and the start and end times of the sag were $k_1^{\text{rms}}$ and $k_2^{\text{rms}}$, respectively. However, by comparing (3) and (15), the computational effort is reduced by using the energy-based method.

### C. Scaling Coefficient Energy-Based Analysis

Taking into account the frequency response of the scaling and wavelet filters as well as the energy decomposition theorem, $\mathcal{E}^s$ is mainly related to the energy of the fundamental frequency component, whereas the $\mathcal{E}^w$ is related to the energy of the high-frequency components of the signal. The energy related to the fundamental frequency component is usually higher than the energy of the high-frequency components of the transients. Therefore, the spectral energy $\mathcal{E} = \mathcal{E}^s + \mathcal{E}^w$ is expected to be similar to the scaling coefficient energy $\mathcal{E}^s$ ($\mathcal{E} \approx \mathcal{E}^s$).

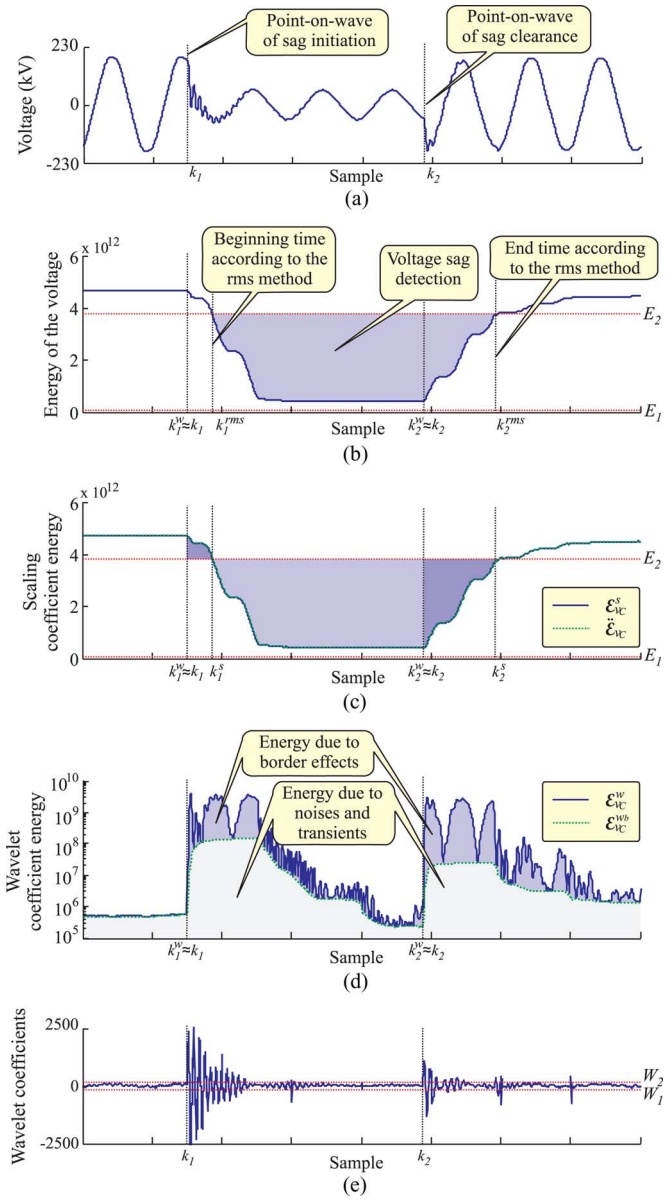


Fig. 4. Actual voltage sag. (a) Phase C voltage: $v_C$. (b) Spectral energy of the voltage: $\mathcal{E}_{v_C}$. (c) Scaling coefficient energies $\mathcal{E}^s_{v_C}$ and $\ddot{\mathcal{E}}_{v_C}$. (d) Wavelet coefficient energies $\mathcal{E}^w_{v_C}$ and $\mathcal{E}^{wb}_{v_C}$. (e) Wavelet coefficients $w_{v_C}$.

The frequency response of the scaling filter changes a little with the mother wavelet. However, at the first scale, the fundamental frequency component is located far from the cutoff frequency of such a filter. As a consequence, the scaling coefficient energies are expected to be little influenced by the mother wavelet.

Fig. 4 depicts the phase C voltage shown in Fig. 2, the respective one-cycle energies $\mathcal{E}_{v_C}$, $\mathcal{E}^s_{v_C}$, $\ddot{\mathcal{E}}_{v_C}$, $\mathcal{E}^w_{v_C}$, and $\mathcal{E}^{wb}_{v_C}$, as well as the wavelet coefficients of $v_C$ ($w_{v_C}$) by using the wavelet Daubechies with four coefficients (db(4)).

According to Fig. 4, during the steady-state system operation ($k < k_1$), $\mathcal{E}_{v_C} \approx 5.10^{12}$, $\mathcal{E}^s_{v_C} \approx 5.10^{12}$, and $\mathcal{E}^w_{v_C} \approx 5.10^5$. In this case, $\mathcal{E}^s_{v_C} \approx 1.10^7 \mathcal{E}^w_{v_C}$. During the voltage sag, $\mathcal{E}^w_{v_C}$ presents a hard increase of energy from the point on wave of sag initiation and recovery. On the other hand, $\mathcal{E}^s_{v_C}$ presents a decrease of energy. However, the maximum value of $\mathcal{E}^w_{v_C}$ is about $4.10^9$

and, in distinct time, the minimum value of $\mathcal{E}^s_{v_C}$ is about $4.10^{11}$ ($\mathcal{E}^s_{v_C} \gg \mathcal{E}^w_{v_C}$). The energy $\mathcal{E}_{v_C}$ is exactly the sum of $\mathcal{E}^s_{v_C}$ and $\mathcal{E}^w_{v_C}$. However, taking into account $\mathcal{E}^s_{v_C} \gg \mathcal{E}^w_{v_C}$, thus $\mathcal{E}_{v_C} = \mathcal{E}^w_{v_C} + \mathcal{E}^s_{v_C} \approx \mathcal{E}^s_{v_C}$. In fact, visually, $\mathcal{E}_{v_C}$ and $\mathcal{E}^s_{v_C}$ presented similar features in Fig. 4(b) and (c), respectively.

In order to demonstrate that the waveforms $\mathcal{E}_{v_C}$ and $\mathcal{E}^s_{v_C}$ in Fig. 4 are quite similar, a square of the correlation coefficient—coefficient of determination $R^2 = 0.99999969$ was obtained by means of a correlational analysis between these energies.

Considering the scaling coefficient energies are quite similar to the spectral energies ($\mathcal{E}^s \approx \mathcal{E}$), it is expected that the scaling coefficient energy analysis may provide similar voltage sag indices to that obtained through the spectral energy. In this case, reference energy ($E^s$) is defined as follows:

$$E^s = \frac{1}{\Delta k} \sum_{m=k_i-\Delta k+1}^{k_i} \mathcal{E}^s(m) \tag{23}$$

where $k_i \geqslant k_x + 2\Delta k - 2$. $E^s = \{E^s_{v_A}, E^s_{v_B}, E^s_{v_C}\}$ are average values in one cycle of $\mathcal{E}^s = \{\mathcal{E}^s_{v_A}, \mathcal{E}^s_{v_B}, \mathcal{E}^s_{v_C}\}$. The system must be in steady-state operation at least in two cycles before $k_i$.

Assuming $\mathcal{E} \approx \mathcal{E}^s$, as an analogy to (21), the residual voltage can also be computed by using $\mathcal{E}^s_{v_A}$, $\mathcal{E}^s_{v_B}$, and $\mathcal{E}^s_{v_C}$ as follows:

$$R_v(k) \approx \sqrt{\frac{\mathcal{E}^s(k)}{E^s}}. \tag{24}$$

A voltage sag can be detected by comparing the scaling coefficient energies of the voltages with the related reference energies, as follows:

$$E_1 E^s \leqslant \mathcal{E}^s \leqslant E_2 E^s \tag{25}$$

for more than a half cycle. Both voltage swells and interruptions are detected if $\mathcal{E}^s \geqslant E_3 E^s$ and $\mathcal{E}^s < E_1 E^s$ for more than a half-cycle, respectively. The samples $k^s_1$ and $k^s_2$ are the start and end times of voltage sags obtained by means of $\mathcal{E}^s$.

## IV. Performance Assessment for the Extraction of Voltage Sag Indices

In order to demonstrate that the scaling coefficient energy-based analysis provides voltage sag indices in accordance with the rms definition with no influence of the power system topology, a database composed of 219 actual records with voltage sags was evaluated. The voltage sags were recorded with various sampling frequencies (from 1.2 to 15.36 kHz) upon 138-, 230-, and 500-kV transmission lines of Brazilian power systems. The voltage sags were due to single-line-to-ground, double-line-to-ground, line-to-line, and three-phase faults. In each actual record, the magnitude (minimum residual voltage termed as sag depth), the start and end times, and duration indices were extracted by means of the energy-based methodologies and compared to the rms definition.

### A. Extraction of Voltage Sag Indices

As expected, the spectral energy-based analysis provided exactly the same indices of the rms-based analysis in all cases.

According to (5), the scaling coefficient energy $\mathcal{E}^s$ proposed in this paper is composed of two components $\mathcal{E}^s = \mathcal{E}^{sa} + \mathcal{E}^{sb}$. The component $\mathcal{E}^{sa}$ is an energy computed with the $L-1$ scaling coefficients influenced by the border effects of the voltage sliding window, whereas $\mathcal{E}^{sb}$ is computed with the last $\Delta k - L + 1$ coefficients of the scaling sliding window and are mainly influenced by the fundamental power frequency component. Disregarding the influence of the border effects ($\mathcal{E}^{sa}$) and expanding the computation of $\mathcal{E}^{sb}$ with all coefficients of the scaling sliding window, [10] proposed $\ddot{\mathcal{E}}$ is the scaling coefficient energy for voltage sag detection. Therefore, $\mathcal{E}^{sb}$ and $\ddot{\mathcal{E}}$ are similar.

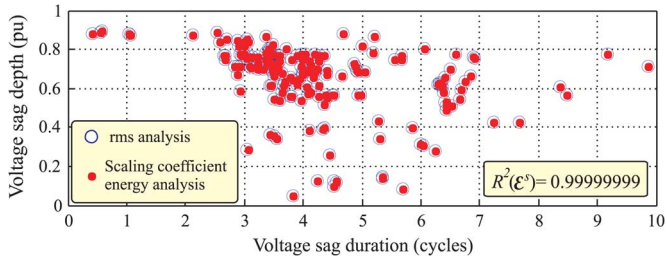


Fig. 5. Extraction of sag indices through $\mathcal{E}^s$ of the MODWT and $v_{\rm rms}$.

TABLE I
Performance Assessment of $\mathcal{E}^s$ and $\ddot{\mathcal{E}}$ of the MODWT

| Mother wavelet | $R^2(\mathcal{E}^s)$ | $R^2(\ddot{\mathcal{E}})$ | $\mu(k^s_1)$ | $\mu(k^s_2)$ | $\mu(\ddot{k}_1)$ | $\mu(\ddot{k}_2)$ |
|---|---|---|---|---|---|---|
| db(2) | 1.0 | 1.0 | 0.0 | 0.0 | 0.5 | 0.5 |
| db(4) | 1.0 | 1.0 | 0.0 | 0.0 | 2.4 | 2.4 |
| db(6) | 1.0 | 1.0 | 0.0 | 0.0 | 4.2 | 4.2 |
| db(8) | 1.0 | 1.0 | 0.0 | 0.0 | 6.0 | 6.0 |
| db(10) | 1.0 | 1.0 | 0.0 | 0.0 | 7.8 | 7.8 |
| db(12) | 1.0 | 1.0 | 0.0 | 0.0 | 9.6 | 9.6 |
| coif(6) | 1.0 | 1.0 | 0.0 | 0.0 | 3.0 | 3.0 |
| coif(12) | 1.0 | 1.0 | 0.0 | 0.0 | 7.0 | 7.0 |
| coif(18) | 1.0 | 1.0 | 0.0 | 0.0 | 11.0 | 11.0 |
| sym(4) | 1.0 | 1.0 | 0.0 | 0.0 | 2.4 | 2.4 |
| sym(8) | 1.0 | 1.0 | 0.0 | 0.0 | 3.0 | 3.0 |
| sym(12) | 1.0 | 1.0 | 0.0 | 0.0 | 5.0 | 5.0 |

db, coif, and sym: Daubechies, Coiflets, and Symlets wavelets.
$L$: Number of coefficients of the wavelet base functions.
$R^2 > 0.9999999$ in all cases.

Fig. 5 depicts the voltage sag depth versus duration obtained through the energy $\mathcal{E}^s$ of the MODWT with db(4) and the rms voltages $v_{\rm rms}$ for all actual voltage sags. $R^2(\mathcal{E})$ is defined as the coefficient of determination as a result of the 2-D correlation analysis of the sag depth versus duration of the rms voltage sag definition with the sag depth versus duration of the energy $\mathcal{E}$. According to Fig. 5, $\mathcal{E}^s$ provided residual voltage and duration according to the definition, because a strong relationship of voltage sag indices from $\mathcal{E}^s$ and the rms voltages was obtained ($R^2(\mathcal{E}^s) = 0.99999999$).

Table I summarizes the performance of the energies $\mathcal{E}^s$ and $\ddot{\mathcal{E}}$ of the MODWT in extraction of voltage sag indices, where $\mu(k_1) = \mu(|k_1 - k_1^{\rm rms}|)$ and $\mu(k_2) = \mu(|k_2 - k_2^{\rm rms}|)$ are the average errors of $k_1$ and $k_2$ with the rms definition, respectively. The same analysis was accomplished for the energy $\mathcal{E}^s$ of the DWT (Table II).

As discussed in the previous section, $\mathcal{E}^s \approx \mathcal{E}$ for all wavelet base functions. This statement was confirmed by means of sta-

TABLE II
PERFORMANCE ASSESSMENT OF THE ENERGY $\mathcal{E}^s$ OF THE DWT

| Mother wavelet | $R^2(\mathcal{E}^s)$ | $\mu(k_1^s)$ | $\mu(k_2^s)$ | Mother wavelet | $R^2(\mathcal{E}^s)$ | $\mu(k_1^s)$ | $\mu(k_2^s)$ |
|---|---|---|---|---|---|---|---|
| db(2) | 1.0 | 0.5 | 0.5 | coif(6) | 1.0 | 0.5 | 0.5 |
| db(4) | 1.0 | 0.5 | 0.5 | coif(12) | 1.0 | 0.5 | 0.5 |
| db(6) | 1.0 | 0.5 | 0.5 | coif(18) | 1.0 | 0.5 | 0.5 |
| db(8) | 1.0 | 0.5 | 0.6 | sym(4) | 1.0 | 0.5 | 0.5 |
| db(10) | 1.0 | 0.6 | 0.6 | sym(8) | 1.0 | 0.5 | 0.5 |
| db(12) | 1.0 | 0.5 | 0.5 | sym(12) | 1.0 | 0.5 | 0.5 |

$R^2 > 0.9999999$ in all cases.

tistical analysis of actual data: according to Table I, voltage sag depth and duration extracted through $\mathcal{E}^s$ and $\ddot{\mathcal{E}}$ of the MODWT are in accordance with the rms definition for all evaluated mother wavelets because a strong relationship ($R^2(\mathcal{E}^s)$ and $R^2(\ddot{\mathcal{E}}) > 0.9999999$) of these sag indices with the definition was obtained in all cases.

With regard to the start and end times of the voltage sags, $\mathcal{E}^s$ of the MODWT provided $k_1^s = k_1^{\text{rms}}$ and $k_2^s = k_2^{\text{rms}}$ for all evaluated wavelets ($\mu(k_1^s)$ and $\mu(k_2^s) = 0$ in Table I). On the other hand, $\ddot{\mathcal{E}}$ of the MODWT was affected by the mother wavelets, presenting waveforms with shifting forward in time. For instance, by using the db(4), $\ddot{k}_1$ and $\ddot{k}_2$ were detected in about two samples after $k_1^{\text{rms}}$ and $k_2^{\text{rms}}$, respectively, where $\ddot{k}_1$ and $\ddot{k}_2$ are the start and end times of voltage sags obtained by means of $\ddot{\mathcal{E}}$. By using a wavelet with many more coefficients, such as the db(12), $\ddot{k}_1$ and $\ddot{k}_2$ were detected in about 9.6 samples after $k_1^{\text{rms}}$ and $k_2^{\text{rms}}$, respectively. Therefore, $\mathcal{E}^s$ presented better performance than $\ddot{\mathcal{E}}$.

The real-time scaling coefficients provide shifting forward in time for long mother wavelets due to the convolution process of the MODWT. Therefore, the energies $\mathcal{E}^{sb}$ and $\ddot{\mathcal{E}}$ also present a shifting forward in time with the mother wavelet because these energies are only computed with the coefficients of the scaling sliding window. However, the component $\mathcal{E}^{sa}$ is compensated with the border effects in order to ensure $\mathcal{E} = \mathcal{E}^s + \mathcal{E}^w$ in all samples. As a consequence, the energy $\mathcal{E}^s$ presents sag magnitude, duration, as well as start and end times for all mother wavelets, in accordance with the rms definition.

The proposed energy analysis is based on the energy decomposition theorem of the wavelet transform ($\mathcal{E} = \mathcal{E}^s + \mathcal{E}^w$), which is also valid for the DWT. Taking $\mathcal{E} \approx \mathcal{E}^s$, $\mathcal{E}^s$ of MODWT and DWT into account may provide energy points to the similar energy waveform. Therefore, $\mathcal{E}^s$ of the DWT may also provide voltage sag indices in accordance with the rms definition. In fact, according to Table II, the $\mathcal{E}^s$ of the DWT presents voltage sag depth and duration in accordance with the definition without influence of the mother wavelet ($R^2(\mathcal{E}^s) > 0.9999999$). However, due to the downsampling by a factor of two, $\mathcal{E}^s$ of the DWT provided $k_1^s$ and $k_2^s$ one sample after $k_1^{\text{rms}}$ and $k_2^{\text{rms}}$, respectively, in about 50% of the analyzed actual records ($\mu(k_1^s)$ and $\mu(k_2^s) \approx 0.5$). Therefore, $\mathcal{E}^s$ of the MODWT presented better performance than the DWT.

### B. Effectiveness of the Real-Time MODWT and DWT

Table III summarizes the floating-point operations (FLOPs), per sampling, performed by means of the real-time scaling and wavelet coefficient energies for various mother wavelets, spectral energy, and rms algorithms. All energies require only addition and multiplication operations in each sampling, whereas the rms voltage requires the same FLOPs of the spectral energy plus a division and a square root operation in each sampling. Addition and multiplication operations were considered to be one FLOP. However, the number of FLOPs to compute a division and a square root is a function of the iterative method for estimating these operations in a specific processor. For instance, a digital signal processor (DSP) usually performs the square root by means of an estimation process followed by two iterations of the Newton–Raphson algorithm. As a benchmark, the TMS320xF2833x DSP performs square root and division operations with 28 and 24 execution time in CPU cycles, respectively. In this paper, it is assumed that the rms algorithm requires about 55 FLOPs.

TABLE III
EFFICIENCY OF THE REAL-TIME ALGORITHMS

| $L$ | Number of FLOPs | | | | | |
|---|---|---|---|---|---|---|
| | MODWT* | | | DWT** | | |
| | $\ddot{\mathcal{E}}$ | $\mathcal{E}^s$ | $\mathcal{E}^s$ & $\mathcal{E}^w$ | $\ddot{\mathcal{E}}$ | $\mathcal{E}^s$ | $\mathcal{E}^s$ & $\mathcal{E}^w$ |
| 2 | 6 | 10 | 14 | 6 | 6 | 10 |
| 4 | 10 | 34 | 38 | 10 | 18 | 22 |
| 6 | 14 | 74 | 78 | 14 | 38 | 42 |
| 8 | 18 | 130 | 134 | 18 | 66 | 70 |
| 10 | 22 | 202 | 206 | 22 | 102 | 106 |
| 12 | 26 | 290 | 294 | 26 | 146 | 150 |
| | $flops\_\mathcal{E}^*$ | | 3 | $flops\_rms^*$ | | 55 |

$L$: number of coefficients of the scaling and wavelet filters;
$flops\_\mathcal{E}$: number of FLOPs to compute $\mathcal{E}$;
$flops\_rms$: number of FLOPs to compute $v_{rms}$;
*: performed every sampling;
**: performed in alternate samplings.

The energy $\mathcal{E}^s$ presented the voltage sag indices in accordance with the rms definition with almost no influence of the mother wavelet. Therefore, a compact wavelet with simple implementation such as the db(4) is a good choice for voltage sag analysis, presenting time consumption equivalent to the rms voltage (Table III). In addition, modern processors perform several million FLOPs per second and the computational efforts of all of them are much less than the time step. Therefore, the processing time criterium might not be a critical task for real-time applications with modern processors. The real advantage of the proposed wavelet-based analysis is the additional information for high-speed sag detection obtained by means of the energy $\mathcal{E}^w$, as addressed in the next section.

## V. POINT ON WAVE OF VOLTAGE SAG INITIATION AND RECOVERY

Though very simple and efficient, rms-based methods can provide errors in estimation of some sag characteristics. For instance, the rms voltage does not immediately drop to a lower value, but takes a while during the transition, and the rms voltage does not immediately recover after the fault [2], [14], which can lead to errors in estimation of sag initiation $k_1^{\text{rms}} > k_1$ and recovery $k_2^{\text{rms}} > k_2$, such as that shown in Fig. 2.

The spectral energy of the voltages can be decomposed into scaling and wavelet coefficient energies ($\mathcal{E} = \mathcal{E}^s + \mathcal{E}^w$). $\mathcal{E}^s$ of the MODWT proved to be useful for the identification of sag magnitude and duration according to the definition, whereas it will be demonstrated in this section that $\mathcal{E}^w$ of the MODWT can provide additional high-speed sag detection and accurate identification of the point on wave of sag initiation and recovery, which are important parameters for power system protection and sag mitigation devices [15], [16].

### A. Wavelet Coefficients

The transition between presag and during-sag voltage contains a large amount of higher frequency components [1], called transients in this paper. According to [2], beyond magnitude and duration, transient inception in both voltages and currents is another fundamental concern for voltage sag characterization. For instance, the point on wave of sag initiation and recovery of the event shown in Fig. 2 are followed by transients.

The wavelet coefficients are quite influenced by the transients during the point on wave of sag initiation and recovery. Recently, papers have been proposing the wavelet coefficients of the DWT for detection of these periods [6], [7]. However, the wavelet coefficients of the MODWT provide faster detection of the transients in real time [12].

According to Fig. 4(e), the wavelet coefficients of the MODWT before $k_1$ presented random values due to electrical noises. However, the coefficients from the point on wave of sag initiation and recovery presented higher values due to the transients. Therefore, the point on wave of sag initiation and recovery can be detected by means of thresholds ($W_1$ and $W_2$) established during the steady-state operation as the average $\pm$ 3$\times$ the standard deviation of the wavelet coefficients [6].

The wavelet coefficients are a good alternatives for high-speed voltage sag detection. However, in critical cases, such as a voltage sag due to a high resistance fault located far from the monitored point, the transients can be very damped and $w$ can be strongly influenced by the choice of the mother wavelet, and the high-speed sag detection can fail.

Fig. 6 depicts the phase A voltage of an actual record with minor voltage sag and very damped transients; the energies $\mathcal{E}^s_{v_A}$, $\mathcal{E}^w_{v_A}$, and $\mathcal{E}^{wb}_{v_A}$; as well as the wavelet coefficients of this voltage by using db(6) and db(20). The voltage was sampled at 5.76 kHz. By using db(6), the wavelet coefficients [Fig. 6(c)] at the point on wave of sag initiation and recovery, at samples $k_1$ and $k_2$, did not present reliable values to be distinguished from the coefficients related to the noises in steady-state operation. With regard to the db(20), the wavelet coefficients [Fig. 6(e)] could not detect the transients at the point on wave of sag initiation and recovery.

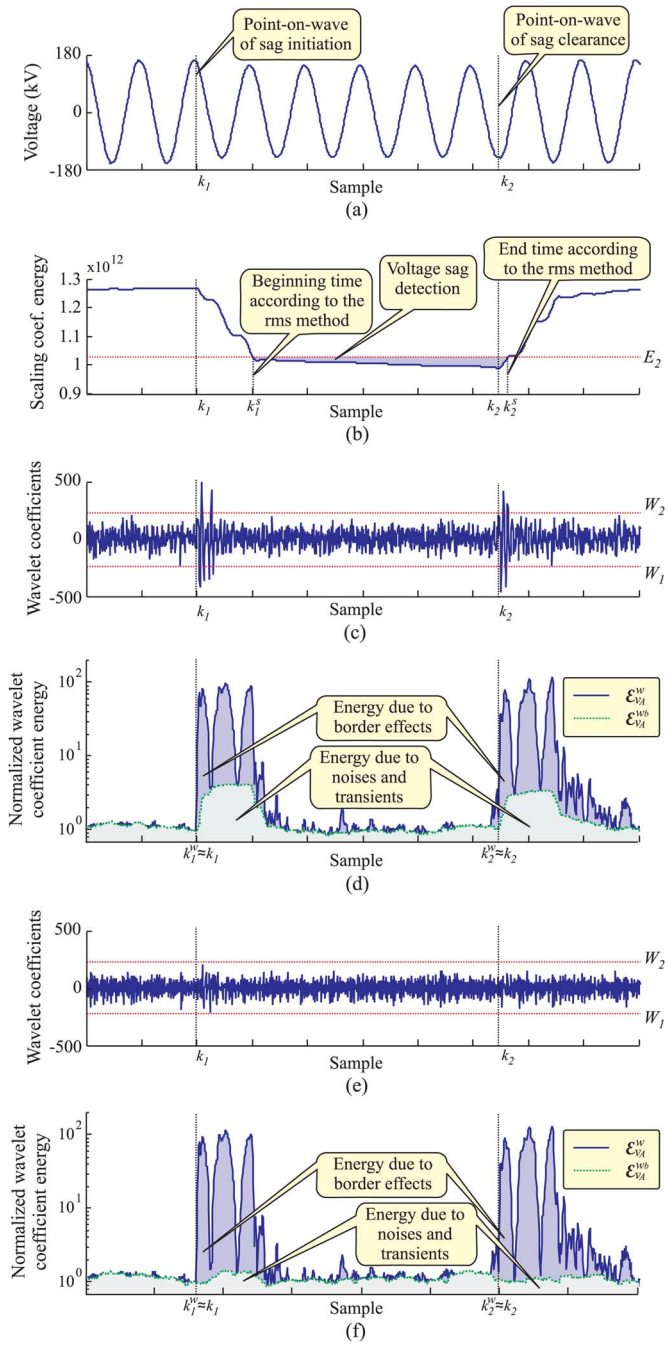


Fig. 6. Actual record with minor voltage sag. (a) Phase A voltage: $v_A$. (b) Scaling coefficient energy: $\mathcal{E}^s_{v_A}$ db(6). (c) Wavelet coefficients—$w_{v_A}$—db(6). (d) Wavelet coefficient energy—$\mathcal{E}^w_{v_A}$ and $\mathcal{E}^{wb}_{v_A}$—db(6). (e) Wavelet coefficients—$w_{v_A}$—db(20); (f) wavelet coefficient energy—$\mathcal{E}^w_{v_A}$ and $\mathcal{E}^{wb}_{v_A}$—db(20).

### B. Wavelet Coefficient Energies $\dot{\mathcal{E}}$ and $\mathcal{E}^{wb}$

The wavelet coefficient energy $\mathcal{E}^{wb}$ is computed with the last $\Delta k - L + 1$ coefficients of the wavelet sliding window. Therefore, $\mathcal{E}^{wb}$ is also influenced by high-frequency noises and transients. According to Fig. 4(d), during the steady-state system operation, $(k < k_1)$ $\mathcal{E}^{wb}_{vC}$ was almost constant. These energy values are due to the high-frequency noises and are assumed to be disturbance free. However, due to the transients, a fast-rising energy occurred from the point on wave of sag initiation and recovery, at samples $k_1$ and $k_2$. A similar wavelet coefficient energy $\dot{\mathcal{E}}$ was used by [10] for real-time detection of voltage sags by using the real-time MODWT. An offline version of $\dot{\mathcal{E}}$ by using the DWT was also used by [8] and [9] for power system disturbance detection.

The energies $\dot{\mathcal{E}}$ and $\mathcal{E}^{wb}$ are also good alternatives for high-speed voltage sag detection. However, these energies, such as the wavelet coefficients, are influenced by the choice of the mother wavelet and can fail in critical cases. For instance, $\mathcal{E}^{wb}_{v_A}$

did not present a sharp increase of energy from samples $k_1$ and $k_2$ in Fig. 6(d) and (f).

### C. Wavelet Coefficient Energies With Border Effects $\mathcal{E}^{wa}$

According to Fig. 1, when the signal sliding window reaches the first sample affected by transients, the real-time wavelet coefficient $w(k)$ is a result of an inner product of the wavelet filter $\tilde{h}$ with the last $L$ samples of the signal, where $L-1$ samples are related to the steady-state operation. As a consequence, an increase in magnitude of $w(k)$ is expected because the last coefficients were only computed with samples during steady-state operation. At the first sample with transients, all of the wavelet coefficients with border effects $\tilde{w}$ are also computed by means of an inner product of $\tilde{h}$ with $L-1$ samples of the steady-state operation and the first sample affected by the transients. Therefore, all coefficients $\tilde{w}$ may also present an increase in magnitude.

In real time, at the first sample with transients, $\mathcal{E}^{wb}$ and $\dot{\mathcal{E}}$ will only take into consideration one wavelet coefficient affected by the transients, whereas $\mathcal{E}^{wa}$ of the MODWT will take into consideration $L-1$ coefficients affected by the transients. Therefore, $\mathcal{E}^{wa}+\mathcal{E}^{wb}=\mathcal{E}^{w}$ may present the sharpest increase of energy during the transient period.

### D. Wavelet Coefficient Energies $\mathcal{E}^{w}$

This paper proposes the real-time wavelet coefficient energies as $\mathcal{E}^{w}=\mathcal{E}^{wa}+\mathcal{E}^{wb}$, which take into consideration the effects of the noise and transients $(\mathcal{E}^{wb})$ as well as the border effects $(\mathcal{E}^{wa})$. For instance, according to Fig. 4(d), $\mathcal{E}^{w}_{v_C}$ during the steady-state system operation $(k<k_1)$ was almost constant (there are no border effects). These energies are due to the high-frequency noises and are assumed to be disturbance free $(\mathcal{E}^{w}_{v_C}\approx\mathcal{E}^{wb}_{v_C})$. However, due to the transients and border effects, fast-rising energy occurred at samples $k_1^w\approx k_1$ and $k_2^w\approx k_2$, where $k_1^w$ and $k_2^w$ are estimations of the point on wave of voltage sag initiation and recovery, respectively, obtained through $\mathcal{E}^{w}$ analysis. The energy $\mathcal{E}^{w}_{v_C}=\mathcal{E}^{wa}_{v_C}+\mathcal{E}^{wb}_{v_C}$ increased faster to a higher value than $\mathcal{E}^{wb}_{v_C}$, which is a good feature for transient detection.

Fig. 7 depicts the wavelet coefficients of the MODWT as well as $\mathcal{E}^{w}_{v_C}$ and $\mathcal{E}^{wb}_{v_C}$ of the voltage shown in Fig. 4(a) for five wavelets: db(4), db(8), db(12), coif(6), and coif(12) in order to show the influence of the mother wavelet in real-time detection of the transients in the point on wave of sag initiation.

The real-time wavelet coefficient $w(k)$ is computed with the last $L$ samples of the original signal, which include the $k$th sample. Therefore, the real-time sample $k$ of the signal is used to compute the $k$th wavelet coefficient and will be used to compute the next $L-1$ real-time coefficients. As a consequence, the transients starting at the $k$th sample can be detectable from the real-time sample $k$ to the future next samples according to the features of the wavelet base functions (e.g., the fault-induced transients started at sample $k_1$ in Fig. 7). By using the wavelets db(4), db(8), db(12), coif(6), and coif(12), the first considerable wavelet coefficient peak was located at samples $k_1$, $k_1$, $k_1+1$, $k_1+1$, and $k_1+3$, respectively. Therefore, there is a shifting forward in time of the wavelet coefficients and the related energy $\mathcal{E}^{wb}$ with long mother wavelets. On the other hand, the energy $\mathcal{E}^{w}$ was less influenced by the choice of the mother wavelet, and

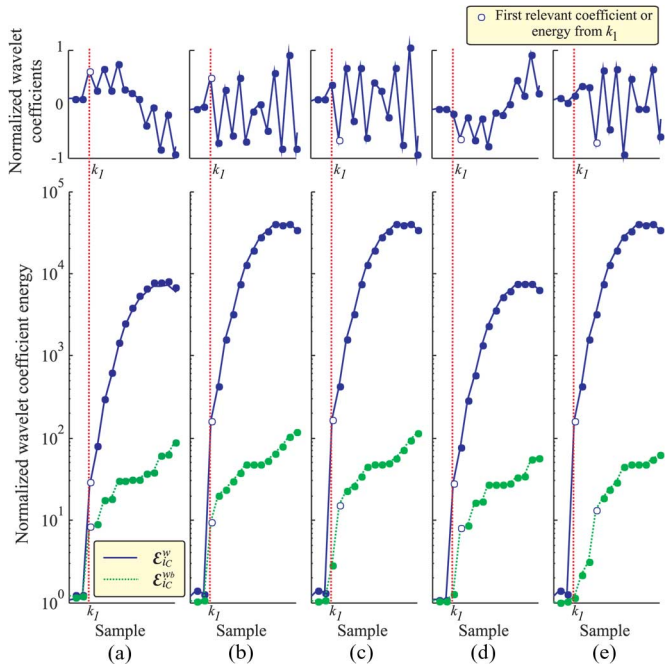


Fig. 7. Wavelet coefficients $w_{v_C}$ and wavelet coefficient energies $\mathcal{E}^{w}_{v_C}$ and $\dot{\mathcal{E}}_{v_C}$: (a) db(4), (b) db(8), (c) db(12), (d) coif(6), (e) coif(12).

the point on wave of sag initiation could be detectable at the first sample with transients in all evaluated mother wavelets (Fig. 7).

The real-time energy $\mathcal{E}^{w}$ presented better performance for point on wave of sag initiation and recovery than both the wavelet coefficients and the energy $\dot{\mathcal{E}}$ because fast (no shifting in time to detect the transients) and accurate (increase of energy for transient detection) detection of these point on waves were accomplished with almost no influence of the mother wavelet, even though in critical cases.

### E. Effectiveness of the Real-Time MODWT and DWT

The proposed MODWT energy analysis is based on the energy decomposition theorem of the wavelet transform, which is also valid for the DWT: $\mathcal{E}=\mathcal{E}^{s}+\mathcal{E}^{w}$ for MODWT and DWT. Therefore, $\mathcal{E}^{w}$ of the DWT may also provide the point on wave of sag initiation and recovery. Fig. 8 depicts the wavelet coefficient energy $\mathcal{E}^{w}$ of the MODWT and the DWT by using the db(4) wavelet of the voltage sag shown in Fig. 4(a). The energy $\mathcal{E}^{w}$ of the DWT is computed in alternate samplings (downsampling process) and the two possible cases were taken into account $\mathcal{E}^{w}$ of the DWT computed in odd samplings [Fig. 8(b)] and $\mathcal{E}^{w}$ of the DWT computed in even samplings [Fig. 8(c)].

According to Fig. 8, the energies $\mathcal{E}^{w}$ of the MODWT and DWT are similar. However, $\mathcal{E}^{w}$ of the DWT can detect the point on wave of voltage sag initiation and recovery either at the same time as the MODWT [Fig. 8(b)] or one sample after [Fig. 8(c)]. Therefore, the real-time detection of the point on wave of voltage sag initiation and recovery is faster by means of the energy $\mathcal{E}^{w}$ of the MODWT.

## VI. Conclusion

This paper presented an energy-based methodology for characterization of voltage sags. The spectral energy of the voltages

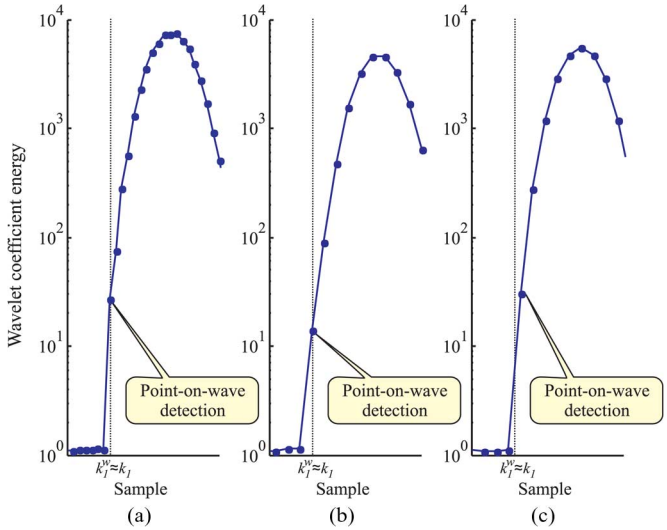


Fig. 8. Effects of the downsampling of the wavelet transform. (a) $\mathcal{E}^w$ of the MODWT. (b) $\mathcal{E}^w$ of the DWT (in odd samplings). (c) $\mathcal{E}^w$ of the DWT (in even samplings).

provided exactly the same voltage sag indices (magnitude and duration) as the rms definition with less computational efforts per sample. However, the point on wave of sag initiation and recovery are not accurately identified by using these techniques.

The spectral energy of the voltages can be decomposed into scaling and wavelet coefficient energies at the first scale with processing time equivalent to the rms voltage computation by using compact mother wavelets. Based on actual data analysis, the scaling coefficient energy provided magnitude and duration of voltage sags according to the definition. However, the wavelet coefficient energy provided additional high-speed detection of the point-on-wave of sag initiation and recovery. Both scaling and wavelet coefficient energies were scarcely affected by the choice of the mother wavelet. The maximal overlap DWT presented better performance than the DWT.

Electrical equipment operates best when the rms voltage is constant and equal to the nominal rms voltage. For example, computers, consumer electronics, induction and synchronous motors, and adjustable-speed drivers are sensitive to reductions in voltage. Some of these electrical devices can stop operating completely in a case of voltage sag. In addition, voltage sag may cause false tripping in protection apparatus. Therefore, the real-time detection of the point of wave of voltage sags by means of the wavelet coefficient energy analysis and the real-time estimation of the residual voltage by means of the scaling coefficient energy analysis can be useful for voltage sag mitigation devices and the protection of power systems.

## APPENDIX
## DESCRIPTION AND DEMONSTRATION ON (13)

From (20), the one-cycle voltage energy can be defined in terms of the one-cycle rms voltage, as follows

$$\mathcal{E}(k) = v_{rms}^2(k)\Delta k. \tag{26}$$

The sample $k_i$ to compute $E$ and $V$ is also the same. In addition, the sliding window to compute both the spectral energies of the voltage and the rms voltages is the same. In this way, from (26) and (19), at sample $k > k_i$

$$\frac{\mathcal{E}(k)}{E} = \frac{v_{rms}^2(k)\Delta k}{\frac{1}{\Delta k}\sum_{m=k_i-\Delta k+1}^{k_i}\mathcal{E}(m)} \Rightarrow \tag{27}$$

$$\frac{\mathcal{E}(k)}{E} = \frac{v_{rms}^2(k)}{\left(\sum_{m=k_i-\Delta k+1}^{k_i}\frac{v_{rms}^2(m)}{\Delta k}\right)}. \tag{28}$$

The variance of the rms voltage $(\sigma^2)$ in one cycle (from $k_i - \Delta k + 1$ to $k_i$) is defined in terms of the arithmetic average of the squared rms voltage and the square of the arithmetic average of the rms voltage, as follows:

$$\sigma^2 = \sum_{m=k_i-\Delta k+1}^{k_i}\frac{v_{rms}^2(m)}{\Delta k} - \left(\sum_{m=k_i-\Delta k+1}^{k_i}\frac{v_{rms}(m)}{\Delta k}\right)^2. \tag{29}$$

Taking into account the steady-state system operation when the reference rms voltage $V$ and the reference energy of the voltage $E$ are computed, from $k_i - \Delta k + 1$ to $k_i$, the variance of the rms voltage tends to zero because a voltage similar to a sinusoidal function with minor distortion is expected. In this way

$$\sum_{m=k_i-\Delta k+1}^{k_i}\frac{v_{\mathrm{rms}}^2(m)}{\Delta k} \approx \left(\sum_{m=k_i-\Delta k+1}^{k_i}\frac{v_{rms}(m)}{\Delta k}\right)^2. \tag{30}$$

Computing $V$ and $E$ during steady-state system operation, from (28) and (30)

$$\frac{\mathcal{E}(k)}{E} \approx \frac{v_{\mathrm{rms}}^2(k)}{\left(\sum_{m=k_i-\Delta k+1}^{k_i}\frac{v_{rms}(m)}{\Delta k}\right)^2} \tag{31}$$

and from (16)

$$\frac{\mathcal{E}(k)}{E} \approx \left(\frac{v_{rms}(k)}{V}\right)^2. \tag{32}$$

Finally, taking into account $V$ and $E$ computed during the steady-state system operation, the residual voltage can be computed with either the rms voltage or the spectral energy of the voltage, as follows:

$$R_v(k) = \frac{v_{\mathrm{rms}}(k)}{V} \approx \sqrt{\frac{\mathcal{E}(k)}{E}} \tag{33}$$

where $k > k_i$.

## REFERENCES

[1] M. H. J. Bollen, *Understanding Power Quality Problems: Voltage Sags and Interruptions*. New York: Wiley, 2000.
[2] M. H. J. Bollen and I. Y.-H. Gu, *Signal Processing of Power Quality Disturbances*. Hoboken, NJ: Wiley, 2006.
[3] *Electromagnetic Compatibility (EMC)—Part 4-30: Testing and Measurement Techniques–Power Quality Measurement Methods*, IEC 61000-4-30, Oct. 2008.
[4] N. S. Tanaboylu, E. R. Collins, and P. R. Chaney, "Voltage dirturbance evaluation using the missing voltage technique," in *Proc. 8th Conf. Harmonics Qual. Power*, 1998, pp. 577–582.

[5] S. Santoso, E. J. Powers, W. M. Grady, and P. Hofmann, "Power quality assessment via wavelet transform analysis," *IEEE Trans. Power Del.*, vol. 11, no. 2, pp. 924–930, Apr. 1996.
[6] A. C. Parsons, W. M. Grady, and E. J. Powers, "A wavelet-based procedure for automatically determining the beginning and end of transmission system voltage sags," *Proc. IEEE Power Eng. Soc.*, vol. 2, pp. 1310–1315, Feb. 1999.
[7] O. Gencer, S. Öztürk, and T. Erfidan, "A new approach to voltage sag detection based on wavelet transform," *Elect. Power Energy Syst.*, pp. 133–140, Jul 2009.
[8] K. M. Silva, B. A. Souza, and N. S. D. Brito, "Fault detection and classification in transmission lines based on wavelet transform and ANN," *IEEE Trans. Power Del.*, vol. 21, no. 4, pp. 2058–2063, Oct 2006.
[9] F. B. Costa, B. A. Souza, and N. S. D. Brito, "Detection and classification of transient disturbances in power systems," *Inst. Elect. Eng. Jpn. Trans. Power Energy*, pp. 910–916, Oct 2010.
[10] F. B. Costa, B. A. Souza, and N. S. D. Brito, "Real-time detection of voltage sags based on wavelet transform," presented at the IEEE/Power Eng. Soc. Transm. Distrib. Conf. Expo.: Latin America, São Paulo, Brazil, Nov. 2010.
[11] D. B. Percival and A. T. Walden, *Wevelet Methods for Time Series Analysis*. Cambridge, U.K.: Cambridge Univ. Press, 2000.
[12] F. B. Costa, B. A. Souza, and N. S. D. Brito, "Real-time detection of fault-induced transients in transmission lines," *Inst. Eng. Technol. Electron. Lett.*, pp. 753–755, May 2010.
[13] *IEEE Recommended Practice for Monitoring Electric Power Quality*, IEEE Standard 1159-1995, Jun 1995.
[14] R. Naidoo and P. Pillay, "A new method of voltage sag and swell detection," *IEEE Trans. Power Del.*, vol. 22, no. 2, pp. 1056–1063, Apr. 2007.
[15] S. Z. Djokic, J. V. Milanovic, and S. M. Rowland, "Advanced voltage sag characterisation ii: Point on wave," *Inst. Eng. Technol. Gen. Transm. Distrib.*, vol. 1, no. 1, pp. 146–154, Jan 2007.
[16] C. Fitzer, M. Barnes, and P. Green, "Voltage sag detection technique for a dynamic voltage restorer," *IEEE Trans. Ind. Appl.*, vol. 40, no. 1, pp. 203–212, Jan./Feb. 2004.

**Flavio B. Costa** (S'05-M'10) was born in 1978 in Brazil. He received the B.Sc., M.Sc., and Ph.D. degrees in electrical engineering from UFCG, Brazil, in 2005, 2006, and 2010, respectively.

He was a Postdoctoral Researcher at UFCG in 2010 on power system protection. Currently, he is a Professor at Federal University of Rio Grande do Norte—School of Science and Technology, Campus Univesitário Lagoa Nova, Natal, Brazill. In 2011-2012, he was a Visiting Researcher at K.U. Leuven, Leuven, Belgium. His research interests include power system protection, electric power quality, renewable energy systems, as well as smart-grid solutions.

Prof. Costa received the 2010 Brazil Engineering Award and 2011 WEG Award in Technological Innovation for his Ph.D. dissertation on real-time analysis of faults and power-quality disturbances.

**Johan Driesen** (S'93–M'97–SM'12) was born in Belgium in 1973. He received the M.Sc. degree and the Ph.D. degree in electrical engineering from K.U. Leuven, Leuven, Belgium, in 1996 and 2000, respectively, on the finite-element solution of coupled thermal electromagnetic problems and related applications in electrical machines and drives, microsystems, and power-quality issues.

Currently he is a Professor at the K.U. Leuven and teaches power electronics, renewables, and drives. In 2000–2001, he was a Visiting Researcher at the Imperial College of Science, Technology and Medicine, London, U.K. In 2002, he was working at the University of California, Berkeley. Currently, he conducts research on distributed energy resources, including renewable energy systems and power electronics and its applications, for instance, in renewable energy and electric vehicles.